

# Purely wavelength- and amplitude-modulated quartz-enhanced photoacoustic spectroscopy

PIETRO PATIMISCO,<sup>1,2</sup> ANGELO SAMPAOLO,<sup>1,2</sup> YVES BIDAUX,<sup>3,4</sup> ALFREDO BISMUTO,<sup>3</sup> MARSHALL SCOTT,<sup>5</sup> JAMES JIANG,<sup>5</sup> ANTOINE MULLER,<sup>3</sup> JEROME FAIST,<sup>4</sup> FRANK K. TITTEL,<sup>2</sup> AND VINCENZO SPAGNOLO<sup>1,\*</sup>

<sup>1</sup>*Dipartimento Interateneo di Fisica, University and Politecnico of Bari, CNR-IFN UOS BARI, Via Amendola 173, Bari, 70126 Italy*

<sup>2</sup>*Electrical and Computer Engineering Department, Rice University, 6100 Main St., Houston TX, 77005 USA*

<sup>3</sup>*Alpes Lasers SA, CH-2072 Saint-Blaise, Switzerland*

<sup>4</sup>*Institute for Quantum Electronics, ETH-Zurich, CH-8093 Zurich, Switzerland*

<sup>5</sup>*Thorlabs, 10335 Guildford Rd. Jessup, MD 20794, USA*

\**vincenzoluigi.spagnolo@poliba.it*

**Abstract:** We report here on a quartz-enhanced photoacoustic (QEPAS) sensor employing a quantum cascade laser (QCL) structure capable of operating in a pure amplitude or wavelength modulation configuration. The QCL structure is composed of three electrically independent sections: Gain, Phase (PS) and Master Oscillator (MO). Selective current pumping of these three sections allows obtaining laser wavelength tuning without changes in the optical power, and power modulation without emission wavelength shifts. A pure QEPAS amplitude modulation condition is obtained by modulating the PS current, while pure wavelength modulation is achieved by modulating simultaneously the MO and PS QCL sections and slowly scanning the DC current level injected in the PS section.

© 2016 Optical Society of America

**OCIS codes:** (140.5965) Semiconductor lasers, quantum cascade; (300.6390) Spectroscopy, molecular; (110.5125) Photoacoustics.

## References

1. J. Hodgkinson and R. P. Tatam, "Optical gas sensing: a review," *Meas. Sci. Technol.* **24**(1), 012004 (2013).
2. B. W. M. Moeskops, S. M. Cristescu, and F. J. M. Harren, "Sub-part-per-billion monitoring of nitric oxide by use of wavelength modulation spectroscopy in combination with a thermoelectrically cooled, continuous-wave quantum cascade laser," *Opt. Lett.* **31**(6), 823–825 (2006).
3. D. S. Bomse, A. C. Stanton, and J. A. Silver, "Frequency modulation and wavelength modulation spectroscopies: comparison of experimental methods using a lead-salt diode laser," *Appl. Opt.* **31**(6), 718–731 (1992).
4. P. Patimisco, G. Scamarcio, F. K. Tittel, and V. Spagnolo, "Quartz-enhanced photoacoustic spectroscopy: a review," *Sensors (Basel)* **14**(4), 6165–6206 (2014).
5. P. Patimisco, A. Sampaolo, L. Dong, M. Giglio, G. Scamarcio, F. K. Tittel, and V. Spagnolo, "Analysis of the electro-elastic properties of custom quartz tuning forks for optoacoustic gas sensing," *Sensor. Actuat. Biol. Chem.* **227**, 539–546 (2016).
6. A. Sampaolo, P. Patimisco, L. Dong, A. Geras, G. Scamarcio, T. Starecki, F. K. Tittel, and V. Spagnolo, "Quartz-enhanced photoacoustic spectroscopy exploiting tuning fork overtone modes," *Appl. Phys. Lett.* **107**(23), 231102 (2015).
7. F. K. Tittel, A. Sampaolo, P. Patimisco, L. Dong, A. Geras, T. Starecki, and V. Spagnolo, "Analysis of overtone flexural modes operation in quartz-enhanced photoacoustic spectroscopy," *Opt. Express* **24**(6), A682–A692 (2016).
8. S. Schilt, L. Thévenaz, and P. Robert, "Wavelength modulation spectroscopy: combined frequency and intensity laser modulation," *Appl. Opt.* **42**(33), 6728–6738 (2003).
9. K. Ruxton, A. L. Chakraborty, W. Johnstone, M. Lengden, G. Stewart, and K. Duffin, "Tunable diode laser spectroscopy with wavelength modulation: Elimination of residual amplitude modulation in a phasor decomposition approach," *Sensor. Actuat. Biol. Chem.* **150**, 367–375 (2010).
10. P. Patimisco, S. Borri, A. Sampaolo, H. E. Beere, D. A. Ritchie, M. S. Vitiello, G. Scamarcio, and V. Spagnolo, "A quartz enhanced photo-acoustic gas sensor based on a custom tuning fork and a terahertz quantum cascade laser," *Analyst (Lond.)* **139**(9), 2079–2087 (2014).

11. P. Zhimin, D. Yanjun, C. Lu, and Y. Qiansuo, "Odd harmonics with wavelength modulation spectroscopy for recovering gas absorbance shape," *Opt. Express* **20**(11), 11976–11985 (2012).
12. P. Kluczynski, J. Gustafsson, Å. M. Lindberg, and O. Axner, "Wavelength modulation absorption spectrometry - An extensive scrutiny of the generation of signals," *Spectrochim. Acta B At. Spectrosc.* **56**(8), 1277–1354 (2001).
13. J. R. P. Bain, M. Lengden, G. Stewart, and W. Johnstone, "An absolute absorption line shapes in tunable diode laser spectroscopy using external amplitude modulation with balanced detection," *IEEE Sens. J.* **16**, 675–680 (2016).
14. P. Kluczynski and O. Axner, "Theoretical description based on Fourier analysis of wavelength-modulation spectrometry in terms of analytical and background signals," *Appl. Opt.* **38**(27), 5803–5815 (1999).
15. S. Schilt and L. Thévenaz, "Wavelength modulation photoacoustic spectroscopy: theoretical description and experimental results," *Infrared Phys. Technol.* **48**(2), 154–162 (2006).
16. Y. Bidaux, R. Terazzi, A. Bismuto, T. Gresch, S. Blaser, A. Muller, and J. Faist, "Measurements and simulations of the optical gain and anti-reflection coating modal reflectivity in quantum cascade lasers with multiple active region stacks," *J. Appl. Phys.* **118**(9), 093101 (2015).
17. A. Bismuto, S. Blaser, R. Terazzi, T. Gresch, and A. Muller, "High performance, low dissipation quantum cascade lasers across the mid-IR range," *Opt. Express* **23**(5), 5477–5484 (2015).
18. Y. Bidaux, A. Bismuto, P. Patimisco, A. Sampaolo, T. Gresch, G. Strubi, S. Blaser, F. K. Tittel, V. Spagnolo, A. Muller, and J. Faist, "Mid infrared quantum cascade laser operating in pure amplitude modulation for background-free trace gas spectroscopy," *Opt. Express*, in press.
19. L. S. Rothman, I. E. Gordon, Y. Babikov, A. Barbe, D. Chris Benner, P. F. Bernath, M. Birk, L. Bizzocchi, V. Boudon, L. R. Brown, A. Campargue, K. Chance, E. A. Cohen, L. H. Coudert, V. M. Devi, B. J. Drouin, A. Fayt, J. M. Flaud, R. R. Gamache, J. J. Harrison, J. M. Hartmann, C. Hill, J. T. Hodges, D. Jacquemart, A. Jolly, J. Lamouroux, R. J. Le Roy, G. Li, D. A. Long, O. M. Lyulin, C. J. Mackie, S. T. Massie, S. Mikhailenko, H. S. P. Muller, O. V. Naumenko, A. V. Nikitin, J. Orphal, V. Perevalov, A. Perrin, E. R. Polovtseva, C. Richard, M. A. H. Smith, E. Starikova, K. Sung, S. Tashkun, J. Tennyson, G. C. Toon, V. G. Tyuterev, and G. Wagner, "The HITRAN2012 molecular spectroscopic database," *J. Quant. Spectrosc. Radiat. Transf.* **130**, 4–50 (2013).
20. V. Spagnolo, P. Patimisco, S. Borri, G. Scamarcio, B. E. Bernacki, and J. Kriesel, "Mid-infrared fiber-coupled QCL-QEPAS sensor," *Appl. Phys. B* **112**(1), 25–33 (2013).
21. K. Duffin, A. J. McGettrick, W. Johnstone, G. Stewart, and D. G. Moodie, "Tunable diode laser spectroscopy with wavelength modulation: a calibration-free approach to the recovery of absolute gas absorption line shapes," *J. Lightwave Technol.* **25**(10), 3114–3125 (2007).
22. H. Chang, J. Chang, Q. Huang, Q. Wang, C. Tian, W. Wei, and Y. Liu, "Immunity to laser power variation in a DFB diode laser based optical gas sensor using a division process," *Sensors (Basel)* **15**(4), 9582–9591 (2015).
23. M. Giglio, P. Patimisco, A. Sampaolo, G. Scamarcio, F. K. Tittel, and V. Spagnolo, "Allan deviation plot as a tool for quartz-enhanced photoacoustic sensors noise analysis," *IEEE Trans. Ultrason. Ferroelectr. Freq. Control* **63**(4), 555–560 (2016).

## 1. Introduction

The combination of single mode emission and fast tunability makes quantum cascade lasers (QCLs) extremely attractive for sensitive trace-gas detection. When these features are combined with modulation techniques, very high detection sensitivities can be achieved [1, 2]. In amplitude modulation (AM), the generation of the signal can be accomplished by switching the laser injection current on and off or employing an optical chopper. In wavelength modulation (WM), the frequency of the laser light is modulated with a periodic function, typically a sine wave. One important advantage of WM is that only the noise centered at the detection frequency and within the detection bandwidth will affect trace-gas measurements. The interaction between the chemical species to be detected and the modulated light leads to the generation of signals at the modulation frequency and its harmonics. Each harmonic of the analytical WM signal can be detected coherently with phase-sensitive detection electronics, such as a lock-in amplifier. For gas sensing techniques based on cavity-enhanced and multi-pass absorption cell, the choice of modulation frequency is often limited by the detector bandwidth. The detection band should be high enough in order to limit  $1/f$  laser noise; however, exceeding 100 kHz is not convenient because the noise has leveled off [3]. In the case of the quartz-enhanced photoacoustic (QEPAS) technique, the modulation frequency should match the resonance frequency of the quartz tuning fork (QTF) or its sub-harmonics [4]. Different QTFs geometries can be designed in order to change the resonance frequency from few kHz up to 100 kHz [5], eventually allowing overtone modes of the QTF to be used [6]. However, resonance frequencies higher than 40 kHz are not suitable

because they may exceed the typical vibration-translational relaxation rates of the gas target [7]. WM is accomplished by dithering the laser injection current by a sine function and this typically results in simultaneous AM and WM, with a phase-shift that is laser-dependent [8]. When a Lorentzian gas absorption line is recovered at the modulation frequency of the laser current ( $1f$ -detection), the acquired signal will exhibit a first harmonic derivative line-shape with a residual amplitude modulation (RAM) contribution, arising from the direct intensity modulation of the laser. This RAM gives rise to a high background signal with a small-superimposed absorption signal [9]. To circumvent this problem, detection at twice the applied modulation frequency ( $2f$ -detection) is preferred. The acquired signal will show a background-free second harmonic derivative line-shape and the effect of RAM appears as a distortion of the line-shape [10]. As a result, both  $1f$ - and  $2f$ - detection fail in the recovery of the Lorentzian gas absorption profile. Several efforts have been done in order to recover the Lorentzian-like lineshape profile. For example, methods using odd harmonics of WM have been proposed [11, 12]. An appropriate choice of the lock-in detection phase is needed as well. Thus, post-processing approaches are required. Recently, a method for recovering absolute absorption line shapes from noisy environments based on pure AM from an external amplitude modulator has been also proposed [13]. Although the overall signal-to-noise ratio is comparable to that of conventional second harmonic WM, the apparatus is quite complex.

In this work, we employed a novel multi-terminal quantum cascade laser (QCL) device that allows modulation of the laser intensity and frequency independently from each other. It is composed of three electrically independent sections: the Gain, the Phase (PS) and the Master Oscillator (MO). The unique characteristics of such a device allow achieving two operating conditions: i) WM with  $2f$ -detection without a RAM contribution and ii) pure AM with direct acquisition of the Lorentzian line-shape of a gas absorption profile. To verify our assumptions, we implemented the QCL as the laser source in a QEPAS-based sensor system and tested it by acquiring a  $\text{N}_2\text{O}$  absorption line at  $1278.10 \text{ cm}^{-1}$ . In the first approach, the MO and PS current are simultaneously modulated, while the DC current of phase section is adjusted in order to keep the optical power constant during modulation, thereby cancelling any RAM contribution. In this manner, a pure wavelength modulation approach is obtained and by adding a voltage signal to the MO section, a QEPAS spectrum with a pure second-derivate Lorentzian function line-shape was obtained. In the second approach only the PS current is modulated, which leads to a modulation of the optical power while the emission wavelength remains constant. With this condition, a pure AM configuration is achieved and a QEPAS background-free Lorentzian line-shape profile was obtained.

## 2. Theoretical aspects of wavelength modulation spectroscopy

When the QCL injection current is dithered by a sine function, the modulation produces changes of the emitted optical power and wavelength, thus leading to combined QCL wavelength modulation and intensity modulation, with a phase difference between the two modulations. Various theoretical descriptions of the QCL current modulation technique have been proposed in the literature [8, 14, 15]. When the laser injection current  $i(t)$  is modulated at an angular frequency  $\omega$ ,  $i(t) = i_0 + \Delta i \cos \omega t$ , the light intensity (or optical power)  $I(t) = I_0 + \Delta I \cos \omega t$  and the instantaneous laser frequency  $\nu(t) = \nu_0 + \Delta \nu \cos(\omega t + \psi)$  are simultaneously modulated. The lock-in amplifier output records the variation of the amplitude (the envelope) of a selected harmonic of the modulation frequency. Higher harmonics are generated due to the nonlinearity in the absorption coefficient  $\alpha[\nu(t)]$  at the center frequency  $\nu_0$ . For  $\Delta \nu \ll \text{FWHM}$  of the absorption profile, all harmonics can be extracted from a Taylor-series expansion of the absorption-line-shape  $\alpha[\nu(t)]$  at  $\nu_0$ , ignoring third- and higher-order terms:

$$\alpha[\nu(t)] = \alpha(\nu_0) + \alpha'(\nu_0) \Delta \nu \cos(\omega t + \psi) + \frac{1}{2} \alpha''(\nu_0) \Delta \nu^2 \cos^2(\omega t + \psi) \quad (1)$$

The laser light transmitted  $I_t$  through a weakly absorbing sample is given by:

$$I_t(t) = (I_0 + \Delta I \cos(\omega t)) \left[ 1 - \alpha(v_0) L - \alpha'(v_0) \Delta v \cos(\omega t + \psi) L - \frac{1}{2} \alpha''(v_0) \Delta v^2 \cos^2(\omega t + \psi) L \right] \quad (2)$$

where  $L$  is the optical path-length. Since  $\cos^2(\omega t + \psi) = 1/2 \{1 + \cos[2(\omega t + \psi)]\}$ , the expression for the  $1f$ -signal  $I_{1f}$  at a frequency  $f = \omega/2\pi$  becomes:

$$I_{1f} = \Delta I \cos(\omega t) - \Delta I \alpha(v_0) L \cos(\omega t) - I_0 \alpha'(v_0) \Delta v \cos(\omega t + \psi) L \quad (3)$$

The first term is the background signal, which is independent of the gas concentration and intensity  $I_0$ , but depends on how  $\Delta I$  varies with  $\Delta i$ . The second term is an absorption-dependent contribution and the third term is the first derivative signal arising from wavelength modulation. The phase of the first derivative contribution is shifted by  $\psi$  from the second term. Thus, even for a small amplitude and frequency modulation, the  $1f$ -signal profile is not a true first derivative of the line-shape, but is distorted by the presence of the second term. The  $2f$ -signal  $I_{2f}$  has the form:

$$I_{2f} = -\Delta I \alpha'(v_0) \Delta v \cos(\omega t) \cos(\omega t + \psi) L + \frac{1}{4} I_0 \alpha''(v_0) \Delta v^2 \cos[2(\omega t + \psi)] L \quad (4)$$

In this case, the first term is due to RAM and is proportional to the first derivative of the absorption, whereas the second term represents the second-derivative term, arising from the wavelength modulation (with a phase difference of  $\psi$  between the terms). Hence, the  $2f$ -signal profile is not a true second derivative of the absorption line-shape, even for a small  $\Delta v$ , but is distorted by a contribution originating from the RAM.

### 3. Characterization of the quantum cascade laser

The structure of the QCL employed in this work is composed of three independent electrically separated sections: a central Gain section, a Master Oscillator (MO) and a Phase section (PS). The QCL active region design is based on a 2-phonons transition. The detailed structure of the layers was presented in Ref [16]. The device was processed to a 6 mm long and 9.5 microns wide buried QCL [17]. An InGaAs layer was grown on top of the active region and used as grating host for the 2.25 mm long MO back section, in order to ensure single longitudinal mode operation. On the top of the InGaAs layer, a 3.3  $\mu\text{m}$  thick n-doped InP cladding was deposited by Metalorganic Vapor Phase Epitaxy (MOVPE). The three independent sections were electrically separated by etching a 1.5 microns deep channel in the n-doped top cladding. The central gain section is 3.00 mm long and is used to pump the laser gain (Gain section). At the front facet, an additional 0.75 mm section is defined in order to control its reflectivity by adjusting the reflection phase (the Phase section). When the current  $i_{MO}$  in the MO section is varied and the phase section current  $i_{PS}$  is kept constant, the frequency of the QCL changes. This is due to the thermal tuning of the Bragg period of the grating. Conversely, when  $i_{PS}$  is varied and the  $i_{MO}$  is kept constant, since the PS contains no grating, the QCL frequency remains constant and output power is modulated. In fact, the PS is used to control the facet reflectivity by adjusting the reflection phase; this has the effect to drastically modify the cavity losses and therefore the output power of the device [18].

Each section was separately controlled by employing three current drivers (ILX Lightwave LDX-3232). When the current  $I_{MO}$  in the MO section is varied and the phase section current  $I_{PS}$  is kept constant, the frequency of the QCL changes. Conversely, when  $I_{PS}$  is varied and the  $I_{MO}$  is kept constant, the QCL frequency remains constant [Ref. 18]. The QCL was operated at a temperature of 10 °C and the Gain section was driven with a fixed current of  $I_G = 800$  mA for all measurements reported in this work. The temperature was controlled by using both a water cooling system mounted below the QCL housing and a temperature controller (Wavelength Electronics, MPT10000). A preliminary spectral

investigation of the continuous-wave (CW) operating QCL emission was performed with  $I_{PS} = 120$  mA and varying  $I_{MO}$  from 532 mA to 580 mA. Figure 1 depicts spectra recorded using a Fourier-transform interferometer (Nicolet 8700, ThermoScientific) in a rapid-scan mode with a spectral resolution of  $0.125 \text{ cm}^{-1}$ . The QCL shows single mode emission in the investigated  $I_{MO}$  current range. In the inset of Fig. 1, the peak values of the spectra are plotted as a function of the MO current. The slope  $0.011 \text{ cm}^{-1}/\text{mA}$  of the linear fit to the spectral data represents the current-tuning coefficient of the QCL source.

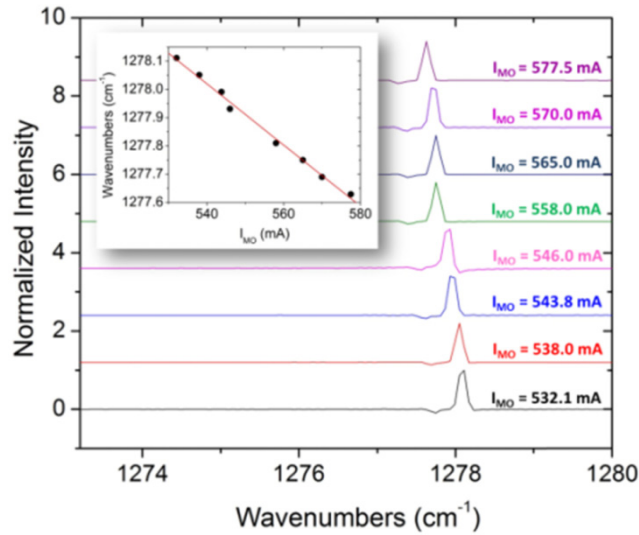


Fig. 1. Emission spectra of the investigated QCL at different MO currents while the injected current in the PS and the Gain section is fixed to 120 mA and 800 mA, respectively. The temperature of the heat sink of the QCL was set to  $10^\circ\text{C}$ . Inset: Peak values of the emission spectra plotted as a function of the MO current. The solid line is the linear fit to the experimental data ( $y = 1283.36 \text{ cm}^{-1} - 0.011 \text{ cm}^{-1}/\text{mA}$ ).

Since the QCL source will be tested for  $\text{NO}_2$  QEPAS detection, we performed a HITRAN based simulation of absorption spectra for a gas mixture consisting of standard air and 10 parts-per-million (ppm) of  $\text{N}_2\text{O}$  at 85 Torr in the spectral range from  $1277.5$  to  $1278.4 \text{ cm}^{-1}$  [19]. Two  $\text{N}_2\text{O}$  absorption lines fall in this spectral range. The strongest absorption line is located at  $1278.10 \text{ cm}^{-1}$  and has a line-strength of  $1.18 \cdot 10^{-19} \text{ cm}^{-1}/\text{mol}$ . No other spectral features are present nearby. To be resonant with the peak value of the selected  $\text{N}_2\text{O}$  absorption line an  $I_{MO} = 532.1$  mA has to be selected. The PS current is scanned from 0 to 150 mA, keeping  $I_{MO}$  fixed. Representative QCL spectra are shown in Fig. 2(a) and the CW QCL-current characteristics are depicted in Fig. 2(b).

The QCL emission wavelength does not change when the current in the QCL PS section is varied, since the MO section current is kept constant. An emitted optical power of 41.4 mW was measured at  $I_{PS} = 120$  mA and  $I_{MO} = 532.1$  mA.



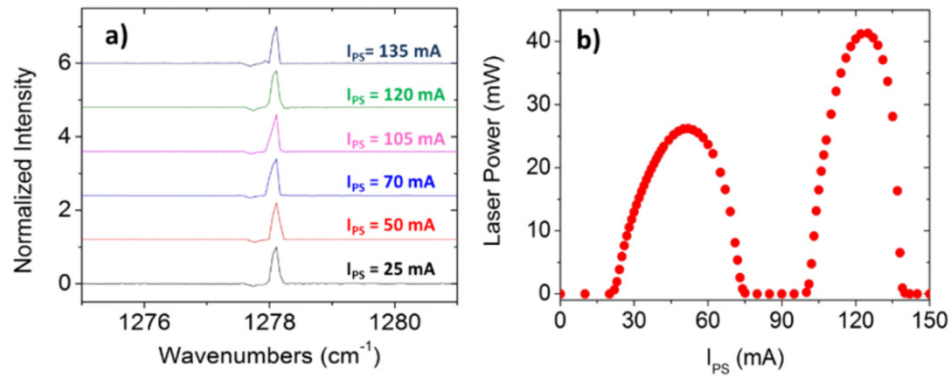


Fig. 2. (a) Representative QCL emission spectra obtained at  $I_{MO} = 532.1$  mA,  $I_G = 800$  mA, and for different  $I_{PS}$  values. No wavelength shift was observed, while  $I_{PS}$  ranges from 20 to 75 mA and from 100 to 140 mA. (b) Optical power emitted by the QCL as a function of the PS current ( $I_{MO} = 532.1$  mA and  $I_G = 800$  mA) measured by means of an infrared detector.

#### 4. Quartz-enhanced photoacoustic spectroscopy based sensor system platform

The QCL was used as the excitation source in a QEPAS set-up depicted in Fig. 3.

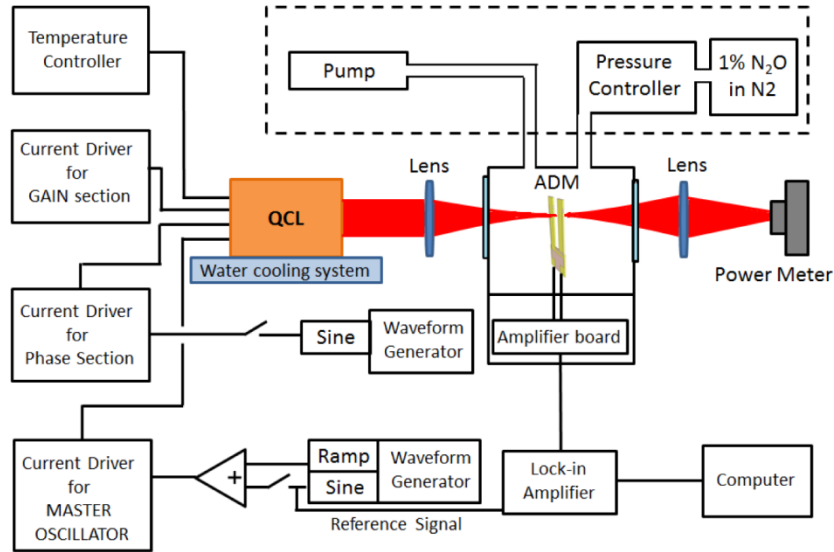


Fig. 3. Schematic of the QEPAS experimental setup employed for the detection of N<sub>2</sub>O in a gas mixture composed of 1% N<sub>2</sub>O in pure N<sub>2</sub>, at a pressure of 85 Torr. QCL – Quantum Cascade Laser. ADM – Acoustic Detection Module.

The QCL output was focused between the prongs of a custom made quartz tuning fork (QTF) using a 1-inch diameter ZnSe lens with 3-12  $\mu\text{m}$  anti-reflection (AR) coating and a focal length of 50 mm. Since the aim of this work is to demonstrate the feasibility to perform pure AM or WM laser spectroscopic measurements, the QEPAS sensing system was kept as simple as possible, avoiding the use of micro-resonators tubes. The prong of the QTF is 17 mm long, 1 mm wide and 0.25 mm thick. The spacing between the two prongs is 0.7 mm [5]. It is crucial that the laser light does not hit the QTF prongs in order to avoid photothermal noise effects [20]. The QTF was enclosed in a compact, vacuum-tight gas cell equipped with two ZnSe windows with a 3-12  $\mu\text{m}$  antireflection coating and gas-in and gas-out connectors,

which constitutes the QEPAS Acoustic Detection Module (ADM). The pressure inside the ADM was controlled by means of a vacuum pump and a pressure controller (MKS, Type 640). The QCL radiation exiting from the gas cell was collected by a ZnSe lens (identical to the input lens) and focused on a power meter for alignment purposes. The QTF signal was detected using a transimpedance amplifier mounted on a circuit positioned close to the ADM and equipped with an electronic switch allowing electrical excitation of the QTF. Representative pictures of the ADM are shown in Fig. 4.

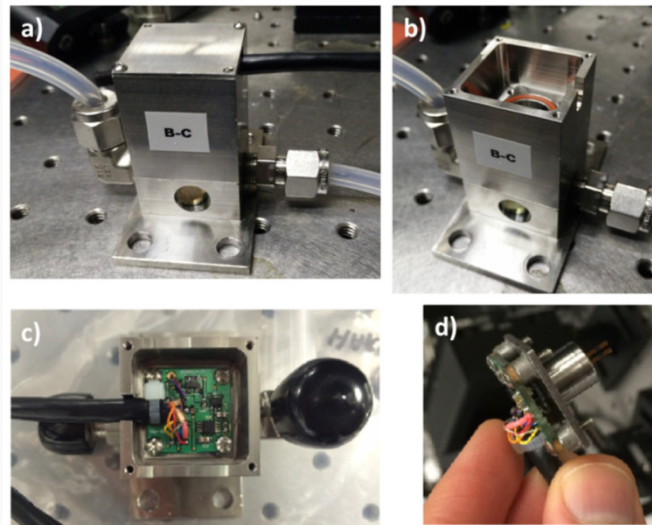


Fig. 4. (a, b) Pictures of the employed ADM. (c, d) Pictures of the transimpedance amplifier circuit mounted inside the housing of the ADM.

This feature was used to determine the main QTF electrical parameters. At a gas pressure of 85 Torr, we measured a resonance frequency  $f_0 = 2871.76$  Hz, an electrical resistance  $R = 482.5$  k $\Omega$  and a quality factor  $Q = 12,400$ . The electrical signal exiting from the circuit was demodulated by means of a lock-in amplifier (DSP, model 7265). Digitalization of the demodulated signal was performed using a National Instruments DAQ Card (USB-6008) and a LabVIEW program was employed for the trace gas measurements. The lock-in integration time was set to 100 ms for all measurements reported in this work. In the WM technique, the lock-in amplifier measures the amplitude of a selected harmonic as a function of time, when the laser center frequency is swept through an absorption line by applying a voltage ramp to the QCL MO section. The time axis is then converted to wavenumbers based on the current-tuning coefficient. A sinusoidal modulation of the laser current can be applied simultaneously (or separately) to the MO and PS sections of the QCL by means of two waveform generators (Stanford Research Systems, model DS345). When the sinusoidal waveform is applied only to the MO section of the QCL, the current modulation induces both a wavelength and optical power modulation. When the current modulation is applied only to the PS section, the modulation induces an optical power modulation, while the emission wavelength remains fixed.

## 5. Pure wavelength modulation and $2f$ signal acquisition

The standard wavelength modulation with  $2f$  signal acquisition was carried out by modulating the current of the MO section at a frequency  $f_0/2 = 1435.88$  Hz, while demodulating the QTF electrical signal at  $f_0$ . The current of the PS section was fixed at 120 mA. A spectral scan of the N<sub>2</sub>O absorption line was obtained by applying a slow voltage ramp to the MO section at a

frequency of 20 mHz. The WM depth must be appropriately selected in order to optimize the sensor performance. Indeed, the WM depth determines the signal strength and the final detection sensitivity of the sensor, as well as influences the line-shape of the spectral scan, which determines the accuracy of the measurements. The optimized current modulation depth that maximizes the  $2f$ -QEPAS signal was 2.7 mA as shown in Fig. 5(a), which corresponds to a wavenumber modulation depth of  $\sim 0.029 \text{ cm}^{-1}$ , close to the  $\text{N}_2\text{O}$  absorption linewidth (FWHM value) of  $0.026 \text{ cm}^{-1}$  at a pressure of 85 Torr. The related modulation index  $m$ , defined as the ratio between the modulation depth and the half-width at half maximum of the absorption profile, is  $\sim 2.2$ , violating the hypothesis of the Taylor-series expansions (see Eq. (1)). However, for such large  $m$ -values, the Taylor series expansion is still applicable to predict the lineshape of different harmonics, but fails in determining the harmonics amplitudes. In fact, as shown in Ref [21], for large  $m$ -values only small distortions arise in the harmonics profiles.

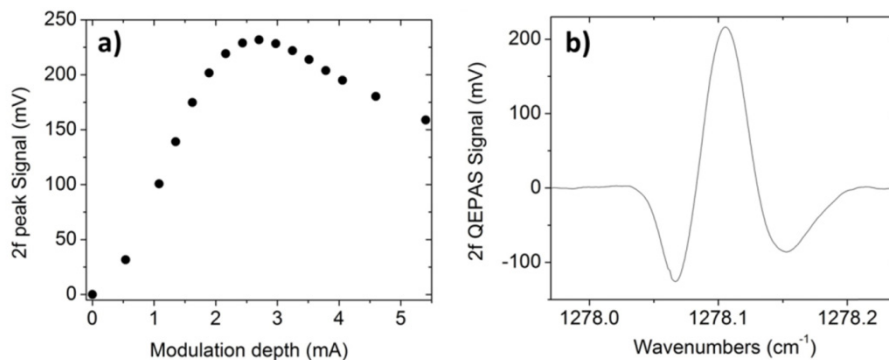


Fig. 5. (a) Peak values of the QEPAS spectral scans acquired using WM and  $2f$ -detection plotted as a function of different modulation depths of the sine waveform applied to the MO section current. (b)  $2f$ -QEPAS spectral scan of the selected  $\text{N}_2\text{O}$  absorption line with the QEPAS sensor operating in the WM mode. The current of the PS section was fixed at 120 mA while both a slow ramp at a frequency of 20 mHz and a sine frequency of 1435.88 Hz and amplitude of 2.7 mA were applied to the MO section. The integration time of the lock-in amplifier was set to 100 ms.

Figure 5(b) shows a representative  $2f$ -QEPAS spectral scan of the  $\text{N}_2\text{O}$  absorption line. The most noticeable feature of the spectral scan is that it is background-free and does not exhibit a pure second derivative line-shape of a Lorentzian absorption profile. A distortion is manifested in the asymmetry of the two negative lobes surrounding the peak. As previously discussed, this asymmetry occurs as a result of RAM that appears in the first derivative of the Lorentzian line-shape (see Eq. (4)). When it is added to the second derivative of the Lorentzian line-shape, the overall effect is to unbalance the two minima. In order to quantify the contribution due to the RAM, we introduced an “asymmetry coefficient”, defined as the difference of the two minima of the profile divided by the mean value of the two minima [22]. The asymmetry coefficient calculated for the spectral scan shown in Fig. 5(b) is 0.376. The RAM term is proportional to the optical power modulation  $\Delta I$  induced by the current modulation  $\Delta i$ , based on Eq. (4). Hence, RAM nulling can be achieved, if  $\Delta I = 0$ . This condition can be realized by adjusting point-by-point the current in the QCL PS section in order to obtain a fixed value of the optical power, while the MO section current varies. Figure 6(a) shows the MO current as a function of the PS section current: for each data point, we measured an optical power of  $P = 29.6 \text{ mW}$  (see inset of Fig. 6(a)). A linear fit was imposed and a slope of  $a = 0.68$  was extracted from Fig. 6(a).



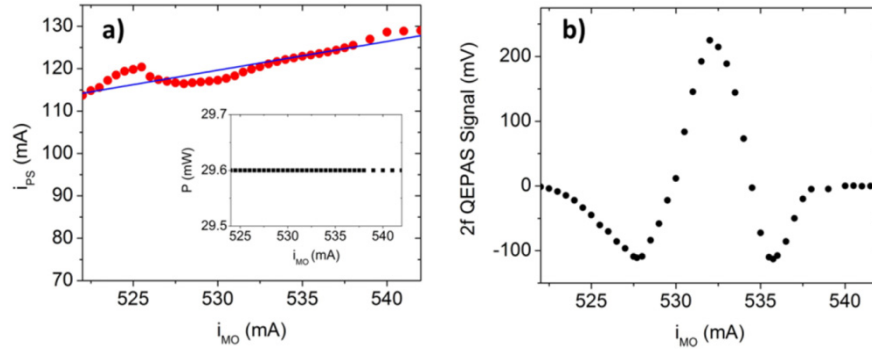


Fig. 6. (a) Current values of the PS section, which maintain the QCL optical power ( $P = 29.6$  mW, see inset) constant as the MO section current varies from 522 mA to 542 mA. The solid line is the linear fit to the experimental data. (b)  $2f$ -QEPAS spectral scan of the selected  $N_2O$  absorption line with the QEPAS sensor operating in a pure WM condition. The current of the PS section was adjusted point-by-point while the MO current varies from 522 mA to 542 mA, by using the calibration data of panel (a). A slow ramp at a frequency of 20 mHz and a sine wave at a frequency of 1435.88 Hz and amplitude of 2.2 mA were simultaneously applied to the MO section; a sine wave at the same frequency and amplitude 1.6 mA was applied to the PS section.

Thus, in our WM experiment, the condition  $\Delta I = 0$  was achieved by applying a sinusoidal dither both to the MO and the PS sections. For this condition, if we denote the amplitude of the MO current modulation by  $\Delta i_{MO}$  and the amplitude of the PS section by  $\Delta i_{PS}$ , the condition  $\Delta I = 0$  is verified only if  $\Delta i_{PS} = a \cdot \Delta i_{MO}$ . Since the optimal current modulation depth is 2.7 mA, the relation  $\Delta i_{PS}^2 + \Delta i_{MO}^2 = 2.7^2$  (in mA units) must also be satisfied. These two relations lead to  $\Delta i_{MO} = 2.2$  mA and  $\Delta i_{PS} = 1.6$  mA. This is only verified if both the sinusoidal dithers have the same initial phase. Figure 6(b) shows a QEPAS spectral scan that is acquired when a sinusoidal dither is applied with a modulation depth of 2.2 mA and 1.6 mA to the MO and PS sections, respectively. The phase section DC current was adjusted point-by-point, while we scanned the MO DC current level. As predicted, the  $2f$ -QEPAS signal shows a second derivative of a Lorentzian line-shape, with a nearly zero asymmetry coefficient ( $\sim 0.016$ ), confirming that the RAM contribution was successfully suppressed.

## 6. Pure amplitude modulation

The only way to obtain a pure AM configuration occurs if the current modulation produces a modulation of the QCL intensity, but no modulation of its wavelength. In the three sections QCL employed in this work, this approach can be accomplished by dithering the PS current with a sinusoidal waveform, while a ramp is applied to the MO section in order to spectrally scan the selected trace gas absorption line. In this case, the current modulation depth of the phase section must be carefully chosen in order to switch between QCL emission-on and -off during each oscillation (see Fig. 2(b)). The optical power becomes zero when the PS current decreases below 100 mA. Therefore, the modulation of the optical power can be approximated by a truncated sine waveform (see inset of Fig. 7).

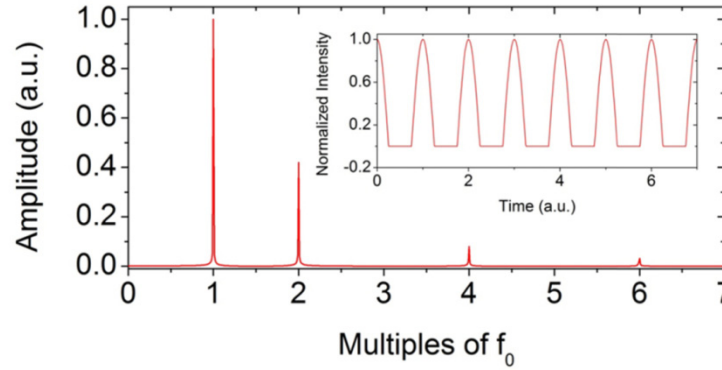


Fig. 7. Fourier transform of a truncated sine waveform at frequency  $f_0$ . Inset: Representative truncated sine function in the time-domain.

Figure 7 shows the frequency-domain spectrum of a truncated sine waveform obtained by Fourier analysis: the strongest harmonic components are the fundamental ( $1f$ ) and the second harmonic ( $2f$ ). Higher harmonics can be neglected. Hence, the optical power modulation can be approximated by:

$$I(t) \propto I_{0,\omega} \cos(\omega t) + I_{0,2\omega} \cos(2\omega t) \quad (5)$$

If the instantaneous laser frequency does not change during the current modulation, from the Lambert-Beer's law we have:

$$I_t(t) \propto [I_{0,\omega} \cos(\omega t) + I_{0,2\omega} \cos(2\omega t)] [1 - \alpha(\nu) L] \quad (6)$$

As result, both the  $1f$ - and  $2f$ -signal will exhibit a pure Lorentzian line-shape. A pure amplitude modulation technique and  $1f$  ( $2f$ ) detection were implemented by applying a sinusoidal dither to the PS section at  $f_0$  ( $f_0/2$ ) and demodulating the QEPAS signal at  $f_0$ . The QCL PS section current was fixed to 120 mA, while a ramp was applied to the MO section current. Similarly, for the WM approach, a preliminary investigation of the influence of the current modulation depth on the QEPAS peak signal was carried out and reported in Fig. 8.

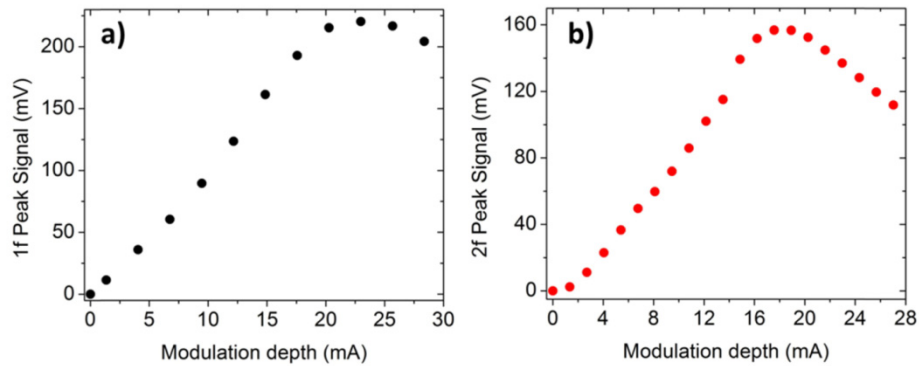


Fig. 8. Peak values of the QEPAS signal acquired with pure amplitude modulation,  $1f$  (a) and  $2f$  (b) detection as a function of the modulation depth of the sine applied to the PS section.

The modulation depths maximizing the QEPAS signal are 23.0 mA and 17.6 mA for  $1f$  and  $2f$  detection, respectively. QEPAS spectral scans obtained for  $1f$  and  $2f$  detection are shown in Fig. 9.

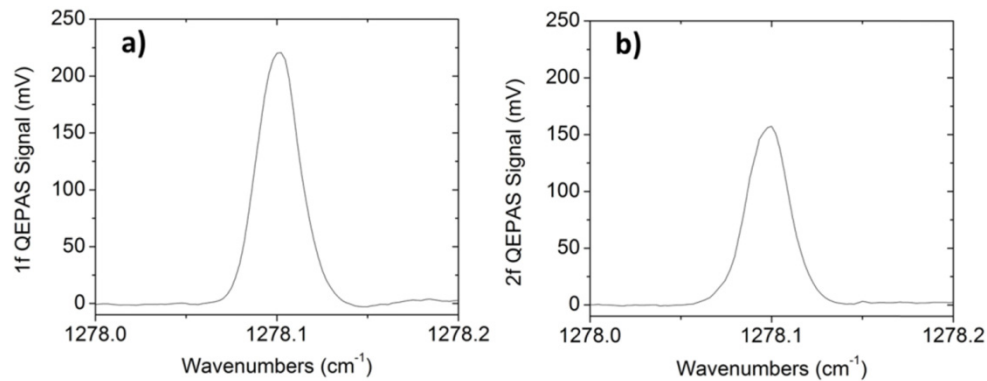


Fig. 9. QEPAS spectral scan of the selected  $\text{N}_2\text{O}$  absorption line with the QEPAS sensor operating in a pure AM condition with  $1f$  (a) and  $2f$  (b) detection. The PS current was dithered with a sinusoidal waveform at a frequency of 2,871.76 Hz and amplitude of 23.0 mA for  $1f$ -detection (a), and at a frequency of 1,435.88 Hz and amplitude of 17.6 mA for  $2f$ -detection (b). A slow ramp at a frequency of 20 mHz was applied to MO section in both cases.

Both  $1f$ - and  $2f$ -QEPAS spectra show a background-free Lorentzian line-shape, demonstrating the achievement of a pure AM condition. The ratio between  $1f$ -peak value and  $2f$ -peak value is 1.40. The FWHM value of both line-shapes is  $0.025 \text{ cm}^{-1}$  (estimated by a Lorentzian fit), close to the FWHM value of the absorption linewidth ( $0.026 \text{ cm}^{-1}$ ).

## 7. Comparison between wavelength modulation and amplitude modulation approaches

Both AM and WM QEPAS techniques were demonstrated to reach a noise background-free condition, using the three sections QCL. The  $2f$ -QEPAS peak signal (216.5 mV) detected with the WM approach is slightly higher than the  $1f$ -QEPAS peak signal (220.1 mV) recorded with the AM technique. However, an estimation of the final detection sensitivity in terms of signal-to-noise ratio for both approaches requires an analysis of the noise level at different signal integration times. This can be accomplished by performing an Allan variance analysis of time sequences of measurements [23], while the QEPAS sensor operates either in pure WM or AM modes. This allows an estimation of the long-terms drift and stability of the QEPAS sensor system. The QCL radiation was locked to the  $\text{N}_2\text{O}$  absorption line peak and the lock-in amplifier time integration was fixed to 100 ms. The measurements were performed continuously for one hour. Both Allan deviation plots are displayed on a log-log graph in Fig. 10. The analysis of Fig. 10 shows that the QEPAS sensor operating in AM mode exhibits an Allan deviation ( $1\sigma$  value) of the noise that is always lower than that achieved for the WM technique. As an example, at an integration time of 10 s, the signal-to-noise ratio of the QEPAS sensor is 2501, when it operates in AM with  $1f$  detection, but drops to 1855 when the WM with  $2f$  detection is employed. This allows us to conclude that, for the experimental conditions described in this work, the amplitude modulation approach with  $1f$  detection is advantageous in terms of the final QEPAS detection sensitivity.

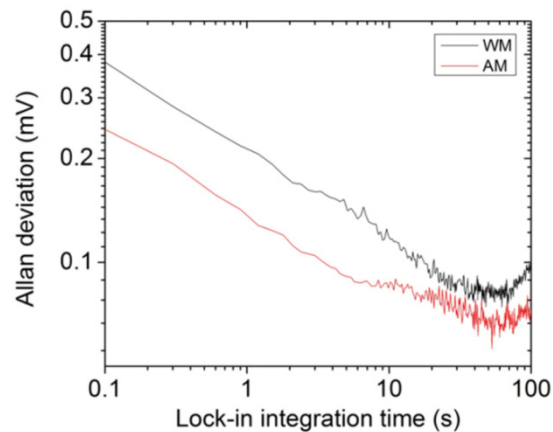


Fig. 10. Allan deviation plot in mV of the QEPAS sensor signal operating in pure AM with  $1f$  detection (red line) and in pure WM with  $2f$  detection (black line) as a function of lock-in integration time.

## 8. Conclusions

In this manuscript, we investigated the potential of a novel QCL structure, composed of three different sections, for gas sensing applications. The structure of the QCL was designed in order to allow modulation of the laser wavelength while the optical power remains constant and, conversely, modulation of the optical power while the wavelength remains fixed. These unique characteristics allow the achievement of both pure amplitude and pure wavelength modulation operating conditions for the realized QEPAS sensor targeting  $\text{N}_2\text{O}$  detection. With pure amplitude modulation and  $1f$ -detection, we recovered the Lorentzian absorption line-shape of the selected  $\text{N}_2\text{O}$  absorption line and measured its full-width-half-maximum value. With pure wavelength modulation and  $2f$ -detection, the residual amplitude modulation contribution was removed and a pure second derivative line-shape of the absorption line was recorded. Finally, an Allan variance analysis of the QEPAS signal shows that a pure AM configuration with  $1f$ -detection is advantageous in terms of signal-to-noise ratio with respect to pure WM with  $2f$ -detection.

## Acknowledgements

Frank Tittel acknowledges support by the Welch Foundation (Grant R4925S). The authors from Dipartimento Interateneo di Fisica di Bari acknowledge financial support from two Italian research projects: PON02 00675 and PON02 00576.